Journal of Applied Physics

RESEARCH ARTICLE | FEBRUARY 15 2024

Understanding melting of Ti crystals with spherical voids from molecular dynamics simulations

Manash Protim Hazarika ; Somendra Nath Chakraborty

J. Appl. Phys. 135, 075101 (2024)
https://doi.org/10.1063/5.0186850

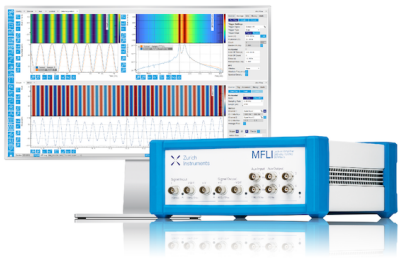

AIP Publishing

Journal of Applied Physics ARTICLE pubs.aip.org/aip/jap

Understanding melting of Ti crystals with spherical voids from molecular dynamics simulations

Cite as: J. Appl. Phys. **135**, 075101 (2024); doi: 10.1063/5.0186850
Submitted: 9 November 2023 · Accepted: 23 January 2024 ·
Published Online: 15 February 2024

Manash Protim Hazarika and Somendra Nath Chakraborty[a)]

AFFILIATIONS

Department of Chemistry, Sikkim University, Gangtok 737102, India

[a)]**Author to whom correspondence should be addressed:** snchakraborty@cus.ac.in

ABSTRACT

Titanium (Ti) is one of the most important metals used in several industrial applications, and the presence of spherical defect reduces its strength and stability. We simulate the melting of Ti crystals with a spherical void of radii 0.6, 0.8, 1.0, and 1.5 nm and also of the crystal without it. Ti is modeled using embedded atom method ,and all crystals are heated at 1 atm from 300 to 2200 K till it melts completely. All molecular dynamics trajectories are analyzed using radial distribution functions, bond-orientational order parameters, Voronoi tessellation, and velocity auto-correlation functions. The results show that 0.6, 0.8, 1.0, and 1.5 nm voids fill before the crystals melt and they fill immediately within few picoseconds; thereafter, atoms rearrange/order to crystal like arrangements, wherein overall crystallinity remains hcp for crystals with 0.6 and 0.8 nm void and changes to bcc for the crystals with 1.0 and 1.5 nm voids. For all crystals with and without void, melting takes place with the loss of both long- and short-range orders and not from liquid like nuclei as proposed by classical nucleation theory.

I. INTRODUCTION

Titanium (Ti) and its alloys are one of the strongest materials used in automobiles, aerospace engineering, defense equipments, pharmaceutical industries, marine industries etc.[1–3] A high strength–weight ratio and corrosion resistant properties make it extremely suitable for several industrial applications. However, the stability and strength of Ti are reduced due to the presence of void defects.[4] Both pressure[5–8] and temperature[9,10] are used to fill these. They also fill up differently depending on pressure, temperature, and the type of interactions present in the crystal. Void closure as a function of compression in Ti crystal is already reported.[4,11,12] During compression, particular slip systems are activated, which lead to dislocations, which decreases with void size. Void closure is also reported for metals such as Mg, Ni, and Cu–Zr.[13–15] This mechanism is also investigated for Lennard-Jones systems and for metals such as Si and Pd.[9,10] In recent years, the melting of high entropy alloys with nanosized voids has been studied.[16,17] In general, defects such as voids, impurities, grain boundaries, and dislocations play an important role during melting, and properties of crystals with these have been widely studied using theoretical as well as experimental techniques.[9,18–22] Out of these defects, voids are of special interest because of their high surface to volume ratio.[5,6,8–10,23] Thus, understanding the melting of crystals with void and the void closure mechanism is extremely significant for metals like Ti, which has applications in several manufacturing industries.

Void closure mechanism has recently been reported by Bai *et al.* for Lennard-Jones (LJ) crystal wherein they show that these voids close in stages. The solid–vapor interface collapses first and populate the void with liquid like particles; thereafter, the solid matrix melts.[9] This kind of melting is also reported in Si. However, in the case of Pd, it was observed that the solid–vapor interface stiffens first and then the matrix liquefies. Both these different melting mechanisms are termed nucleating and non-nucleating.[10] Nucleating mechanism (NM) refers to the melting of the void first and then the crystal. On the other hand, non-nucleating mechanism (NNM) refers to the stiffening of the void skin first and the voids fill when the crystal melts. An unified picture of these mechanisms was also presented, where it was shown that differences between solid–liquid, liquid–vapor, and solid–vapor interfacial energies decide whether NM or NNM takes place in a system.[10] In our earlier study, we have shown that Cu with a spherical void of 1.0 nm, melts NM way; i.e., void is filled and the matrix melts.[23] So the void fills first, and then, the crystal melts. However, between

the melting of the void and the crystal, it amorphizes. For metals with high cohesive forces and melting temperature, the closure of the void is different from simple systems like Lennard-Jones. Moreover, earlier findings have also established that the melting temperature decreases with an increase in the volume fraction.[5,9,23–25] Thus, the presence of voids also reduces the superheating limits of the metal.

Melting in general is a difficult phenomenon to understand. Mechanisms such as Lindemann[26] or Born criteria[27] are used to describe it. Apart from these rules, classical nucleation (CNT) theory is also used to understand it.[28,29] As CNT suggests, solid–liquid/solid–vapor surfaces act as liquid nucleating sites and melting initiated from them. Melting is, thus, facilitated due to the presence of voids in it. However, this simple picture was challenged in a recent study[30] where the role of multiple metastable paths and barriers were shown to be significant for the melting phenomenon. Whatever facilitates melting or whichever transition paths are obtained, it must be noted that surfaces play the central role in melting of crystals.[31] Most importantly, the surface undergoes a transition wherein a layer of the disordered phase between the free surface and the bulk solid is present.[32] In recent literature, role of surface has also been studied using phase-field methods.[33,34] In these studies, the role of voids and, specially, the role played by the width of the void surface interface is underlined. All these studies indicate that understanding melting in general and the effect of void on the melting of metals in particular is also of great significance.[5,9,10,23,25,35,36]

Along with melting with spherical void in a titanium crystal, we also focus on the high temperature hcp to bcc transition in Ti. Ti has three stable polymorphs —namely hcp (α), bcc (β), and hexagonal (ω). At 1 bar and 1155 K, hexagonally close packed (α) Ti transforms to the bcc phase (β). This high temperature hcp–bcc transition is extensively reported in the literature from phonon dispersion studies.[37–40] It is also reported that the presence of defects such as screw dislocations,[41] stacking faults, and twin-boundaries[42] facilitate solid–solid phase transition. Compared to line defect mediated transitions, spherical void mediated transitions are not so well reported. It is quite likely that spherical void can mediate solid–solid transition, specially hcp to bcc. In fact in our simulations of Ti with 1.0 and 1.5 nm spherical void, we observe hcp to bcc transition.

Melting of titanium crystal with spherical voids is hugely significant for its preparation and applications. High temperature hcp to bcc transition is also relevant for knowing the strength and stability of titanium. Studying melting with defects like spherical voids also help us to identify the microscopic level picture associated with melting and to validate or improve theories like CNT with which it is described. Molecular simulations provide us with important physical insights of crystal melting. We, thus, simulate single crystals of Ti with a spherical void of different radii—0.6, 0.8, 1.0, and 1.5 nm. We show that these crystals also melt NM way (void fills and then crystals melt); however, the reorganization of the atoms after the closure plays a central role in maintaining the crystallinity of Ti. Here, in our study, we, thus, show how the reorganization of atoms is relevant before it melts. This is different from the melting or stiffening[10] of the solid–vapor interface. We also focus on how the void properties such as surface area, volume, and structural properties of the first layer of atoms change with time during its filling. First, we report the changes in thermodynamic and structural properties due to the melting of the Ti crystal. Next, we report the dynamics of the void closure. Finally, we analyze the structural rearrangement of the surface atoms and show that crystallinity in these atoms is not lost till the entire crystal melts.

II. METHODOLOGY

A. Simulation details

All our molecular dynamics simulations of Ti are performed using LAMMPS (Large-scale Atomistic/Molecular Massively Parallel Simulator) software package.[43] Titanium is modeled here using the embedded atom potential. This potential was first proposed by Dow and Baskes in 1987,[44] and it has been successfully used to simulate metallic systems such as Cu, Ni, and Pb. Each atom in this potential is embedded in a host of electron gas generated by all surrounding atoms. The amount of energy needed to put one atom into the electron gas of a given density is called the embedding function, which considers many atom effects. In a simulation, the potential energy of an atom, i, is given by

$$E_i = F_\alpha\left(\sum_{i\neq j}\rho_\beta(r_{ij}) + \frac{1}{2}\sum_{i\neq j}\phi_{\alpha\beta}(r_{ij})\right), \quad (1)$$

where r_{ij} is the distance between atoms i and j, $\phi_{\alpha\beta}$ is a pair-wise potential function, ρ_β is the contribution to the electron charge density from atom j of type β at the location of atom i, and F is an embedding function that represents the energy needed to put atom i of type α into the electron cloud. Ackland modified the original Dow and Baskes EAM potential for Ti simulations.[45] In a latter study, Jiang *et al.* showed that hcp Ti modeled by this potential melts at 1941 K.[46] However, in a recent study by Mendelev *et al.*, a new EAM based potential was developed and the hcp–bcc transformation was located using thermodynamic integration techniques and the lattice-switch Monte Carlo method.[47] With these advanced sampling techniques, it was shown that hcp Ti transforms to bcc at 1155 K and then bcc Ti melts at 1918 K. We use this variant of EAM potential developed by Mendelev in our simulations.

We perform our MD simulations at 1 bar and in the temperature range 300–2200 K, under isothermal–isobaric conditions. A Nosé–Hoover barostat was used to control pressure fluctuations during the simulations. It is based on the constant temperature method proposed by Anderson.[48] To control the temperature, we use the Nosé–Hoover thermostat introduced by Nosé[49] and developed by Hoover.[50] Verlet's algorithm[51] with an integration timestep of 2 fs is used to integrate the Newton's equation of motion.

In 12 × 12 × 12 unit cell of bulk HCP Ti with 6912 atoms, we create spherical void of radii 0.6, 0.8, 1.0, and 1.5 nm separately within each of the bulk Ti crystal. We simulate a void free crystal of similar lattice dimensions. We also simulate a crystal with a 1.5 nm void, consisting of 12 700 atoms. We report these results in Fig. S11 in the supplementary material and note that results from this system are comparable with the crystal with 6912 atoms.

All of these are simulated with periodic boundary conditions between 300 and 2200 K. During heating, at each temperature, we equilibrate the system for 5 ns wherein the last configuration from

the previous temperature is used as the initial configuration for the next higher temperature. We use two different temperature intervals to heat the system—between 300 and 900 K, we increase the temperature by 200 K, between 900 and 2200 K and we increase it by 100 K. Heating the system and equilibrating it at higher temperatures is a conventional method used in MD simulations. However, heating rates or ramps are also used to increase the temperature of the system. Temperature is gradually increased per picosecond during these MD simulations. Recent studies have shown that heating rates have an insignificant effect on the melting process and melting temperatures increase marginally with increase in the heating rates.[46] After appropriately equilibrating our system at each temperature, we analyze 5000 configurations dumped at an interval of 0.2 ps. We report the potential energies from the equilibration run at all these temperatures in supplementary material section (Fig. S1). All our systems equilibrated well within 5 ns. Interestingly, we do not observe hcp–bcc transition for the 0.6 and 0.8 nm void system—these systems melt similar to the bulk defect free system.

Choice of the void radii is based on earlier simulation studies—where changes in the melting temperature as a function of void are reported. Most simulation studies use void sizes of radii 0.4≈ 2.5 nm.[5,10] It is also reported that systems with void size 1.7 nm are not stable at room temperatures.[5] Figure 1 schematically shows the titanium crystal with a spherical void. All trajectories are analyzed at different temperatures using bulk density, Lindemann index, coordination number, Q_6 bond-orientational order parameter, radial distribution functions (RDF), and Voronoi Tessellation technique. We also used the common neighbor analysis (CNA) provided by OVITO software[52] to distinguish between hcp, bcc like atoms. Details of the structural analysis performed are presented in Sec. II B.

B. Structural and dynamical analysis

Structural metrics used to analyze the heating trajectories are discussed here. Radial distribution functions (RDFs) are the most important structural quantities, which measure the overall crystallinity of the system. RDF ($g(r)$) is defined as the ratio of the relative probabilities of finding two particles separated by a distance r in a liquid and in an ideal gas.[53] For a monoatomic system, it is defined as

$$g(r) = \frac{V}{N^2} < \sum_{i=1}^{N} \frac{n(r)}{4\pi r^2 \Delta r} > , \tag{2}$$

where V and N are the volume and number of particles in the system, respectively, and $n(r)$ is the number of atoms in the thickness of Δr at the radius of the particle. The nearest neighbors of a central titanium atom, thus, collected (n) within the first minimum of the RDF at every temperature form the coordination number for the centrally located atom.

Structural melting temperature is often defined by root mean square fluctuations in distances, called the Lindemann index δ.[54] The Lindemann index of each atom and of the entire bulk system is calculated using.[55]

$$\delta_i = \frac{1}{N-1} \sum_{j \neq i} \frac{\sqrt{< r_{ij}^2 >_T - < r_{ij} >_T^2}}{< r_{ij} >_T}, \tag{3}$$

$$\delta = \sum_i \delta_i, \tag{4}$$

where N is the number of atoms. δ_i and δ are the Lindemann indices of the ith atom and bulk, respectively, and r_{ij} is the distance between the ith atom and jth atom.

Bond-orientational order parameters were introduced by Steinhardt.[56] These spherical harmonics based order parameters measure the degree of crystallinity of the solid[57] and have been used extensively to characterize melting and freezing transitions.[58,59] Spherical harmonics (Y_{lm}) are obtained using

$$\bar{Y}_{lm} = \frac{1}{nnn} \sum_{j=i}^{nnn} Y_{lm}\left(\theta(r_{ij}), \phi(r_{ij})\right). \tag{5}$$

Here, θ and ϕ are the standard spherical polar angles and Y_{lm}s are summed over the nearest neighbors to the central atom. Then, the rotationally invariant Q_l (for l = 6) is obtained using[56]

$$Q_l = \sqrt{\frac{4\pi}{2l+1} \sum_{m=-l}^{m=l} \bar{Y}_{lm} \bar{Y}_{lm}^{*}}. \tag{6}$$

Voronoi tessellation technique (VT) based polyhedra analysis is used recently to perform structural analysis of crystals, melts, clathrate hydrates, and glasses.[60–64] Voronoi polyhedra of a reference point in a collection of points is the locus of all points that are closest to this point than any other. Topological properties of the polyhedra are the number of faces, edges, and vertices. Here, we analyze the volume, surface, faces, and edges of the polyhedra

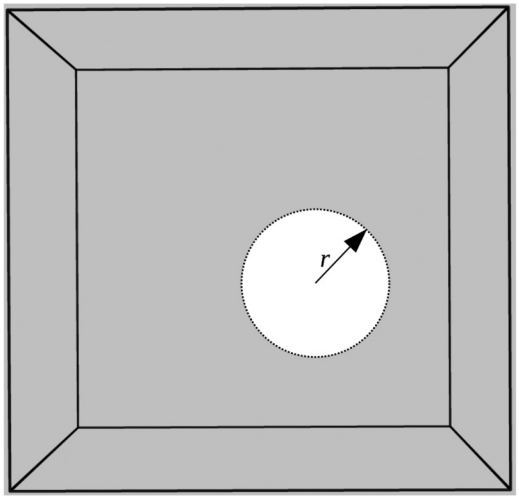

FIG. 1. Schematic of solid matrix with a void of radius r.

obtained from tessellating the three-dimensional space around each Ti atom. All tessellations were performed using the open source Voro++ and Vorotop software.[65,66]

To characterize the local arrangement of atoms, we also take the help of adaptive common neighbor analysis (a-CNA),[67] an extension of the common neighbor analysis (CNA) method[68] available in open visualization tool OVITO. This method is widely used to distinguish between various local structures, in particular between atoms in fcc, hcp, bcc, and icosahedral environments.[69]

All these structural metrics discussed above gives us the overall crystallinity of the system as a function of temperature. However, features of polyhedra distinguish between different—hcp/bcc/distorted hcp/bcc like arrangements. Recently, a Voronoi polyhedra based analysis has been reported where authors identify short-ranged icosahedral orders as precursors to the formation of the bcc phase in molten iron.[70] Apart from VT, we used local Q_6 and the coordination number to analyse the atoms occupying the first layer around the spherical voids. Here, from the center of void, atoms lying at a distance greater than the void radius but within first and second minima of RDF are used to collect the first layer of atoms, respectively. This analysis specifically identifies the rearrangement within the first layer atoms, which is, otherwise, not possible from the VT analysis. Voronoi polyhedra features of these few atoms are difficult to characterize.

Velocity auto-correlation functions (VACFs) of the first layer of Ti atoms were simply obtained using

$$c^{\alpha}(t) = \langle \alpha_i(t)\alpha_i(0)\rangle / \langle \alpha_i(0)\alpha_i(0)\rangle, \tag{7}$$

where α is titanium atom's velocity. Thereafter, relaxation times (τ) were obtained by exponential ($\exp(-t/\tau)$; t = time) fitting to the positive values of ACF peaks (maxima).

III. RESULTS AND DISCUSSION

We perform the MD simulations of Ti crystals with a spherical void of 0.6, 0.8, 1.0, and 1.5 nm and also of the crystal without the void. We first discuss the melting of these crystals from changes in thermodynamic properties and radial distribution functions. Thereafter, we show how much time it takes for the voids to fill and also show that void fills before the crystal melts. Finally, we discuss how the first layer rearranges while the void fills. These results are reported from orientational order parameters, Voronoi analysis, and velocity autocorrelation functions of the surface atoms.

A. Melting of the crystals

In Fig. 2, we show the changes in thermodynamic properties as a function of temperature. Titanium crystal with 0.6 and 0.8 nm spherical void melts between 1900–2000 K and 1800–1900 K, respectively. Similarly void free crystal melts between 2000 and 2100 K. Thermodynamic melting temperature of this potential is 1765 K.[47] Void free crystal is superheated and melts at a higher temperature compared to its melting point. Crystal with the smaller void (0.6 nm) melts at a higher temperature compared to the larger one (0.8 nm). Density, Lindemann index, Q_6, and coordination number change sharply between these temperatures only. The

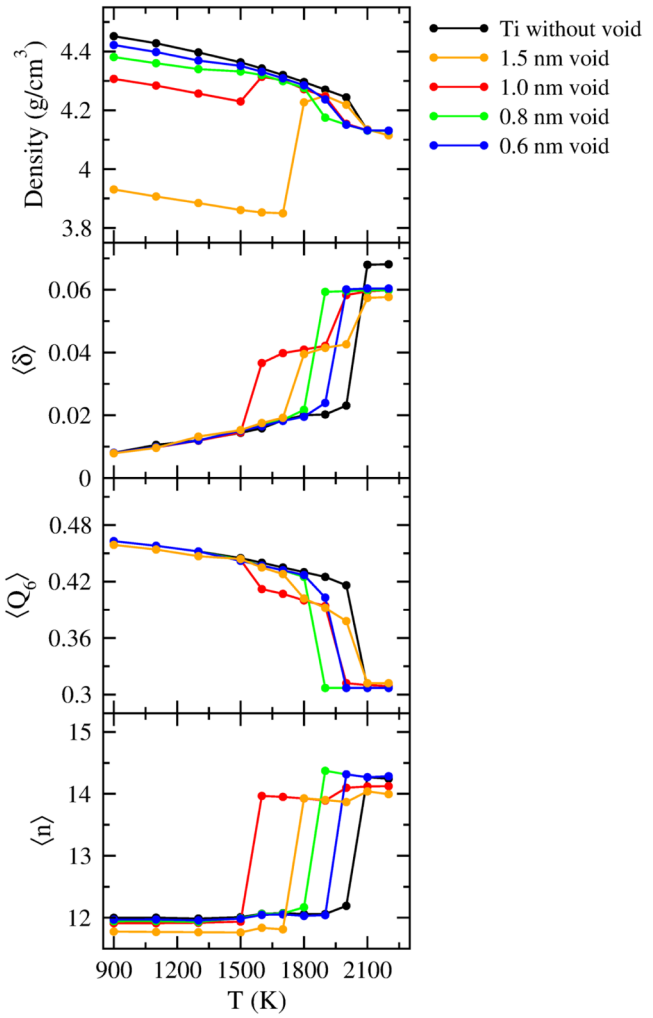

FIG. 2. Density, Lindemann index (δ), bond-orientational order parameter (Q_6), coordination number (n) as a function of temperature.

Lindemann rule predicts that the crystal will melt if the root mean squared displacement of atomic positions exceeds a threshold value. Typically, this value varies between 5% and 20%, depending on the crystal structure, interparticle interactions etc.[71] According to this rule, crystals with 0.6 and 0.8 nm voids melt between 1900–2000 K and 1800–1900 K, respectively. Similarly, the void free crystal melts between 2000 and 2100 K. However, for the crystals with 1.0 and 1.5 nm void, sharp changes in crystal properties occur between 1500 and 1600 K, 1700 and 1800 K and also between 1900 and 2000 K, 2000 and 2100 K. Lindemann parameter changes by 25% and 15% at these two transitions. 25% RMSD change, which takes place between 1500 and 1600 K (for 1.0 nm) and also between 1700 and 1800 K (for 1.5 nm), increases the density of Ti by 1%–2%. We can expect that solid–solid transition takes place before this crystal actually melts. Moreover, Lindemann measures,

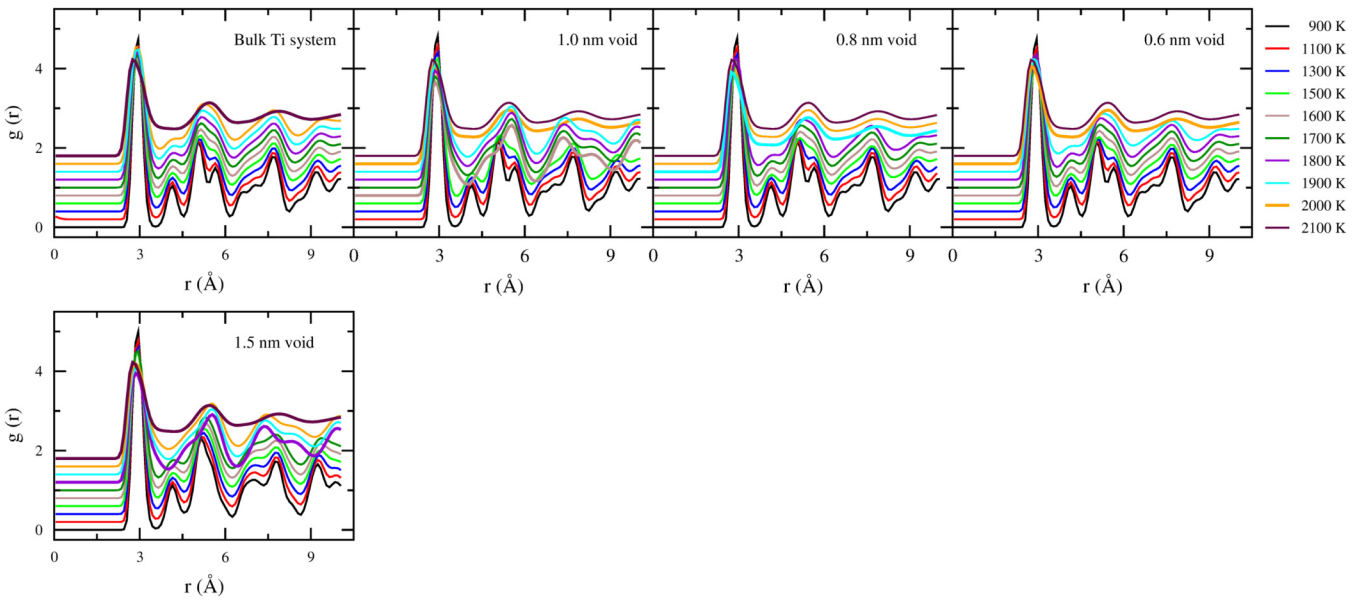

FIG. 3. Radial distribution functions of Ti with 1.5, 1.0, 0.8, 0.6 nm void and void free Ti during melting.

might not be applicable to crystals with defects wherein RMSD change in atomic positions result in another solid polymorph rather than liquid. Structural changes are also understood from radial distribution functions, we report them next in Fig. 3. For the crystals with 0.6 and 0.8 nm void and also for the void free crystal, melting takes place between 1900–2000, 1800–1900, and 2000–2100 K, respectively.

But for the 1.0 and 1.5 nm spherical void system, RDF changes significantly between 1500 and 1600 K, 1700 and 1800 K and also between 1900 and 2000 K, 2000 and 2100 K. For rest of the crystals which melt directly from hcp—in them the second peak at 4 Ådisappears completely by 2100 K.

However, for the crystals with 1.0 and 1.5 nm spherical void—this second peak intensity does not decrease continuously with temperature, but it transforms to a shoulder of the third peak. Disappearance of the second peak confirms the melting of hcp crystal, but the transformation of this peak to a shoulder confirms the transformation of the hcp to bcc phase. In fact for a pure crystal, the position of this second peak distinguishes between the hcp and the bcc phase. We report the RDF of pure crystals in Fig. S2 in the supplementary material—where the second peak of the hcp and bcc crystal appears at 4 and 4.7 Å, respectively. Snapshots, Voronoi polyhedra, and fraction of atoms obtained using OVITO and voro++ are reported in Figs. S3–S9 in the supplementary material, they also confirm that crystals with 1.0 and 1.5 nm void transform to bcc before it melts. Fraction of bcc atoms transformed at 1600 (for 1.0 nm) and 1800 K (1.5 nm) is close to 50%. This fraction of bcc atoms keep the crystal ordered till it melts. Radial distribution functions nicely capture both solid–solid and solid–liquid transition. Solid–liquid transition is characterized by the disappearance of both short- and long-range order in the crystal. Solid–solid transition is characterized by the changes in the long-range order of the atoms. Short-range order is the local crystal like arrangement of the atoms in its immediate neighborhood (first shell). Long-range order is the ordered arrangement of atoms, which translate through the entire crystal. When the solid melts both long- and short-range order disappears. We also show later that the disappearance of order within the first shell is crucial in the melting of crystals.

Figures 2 and 3 show that for crystals with 0.6, 0.8 nm spherical void and also for the void free crystal, melting takes place directly from hcp phase between 1900 and 2000, 1800 and 1900, and 2000–2100 K, respectively. Our findings also confirm the earlier results that voids reduce superheating limits of the crystal.[25] However, the crystals with 1.0 and 1.5 nm spherical void changes first to bcc and then bcc melts to liquid. We obtain the temperatures at which the voids fill from plots of number of atoms inside the spherical void as a function of temperature in Fig. 4. We note that 0.6, 0.8, 1.0, and 1.5 nm spherical voids are filled between 1300–1400, 1400–1500, 1500–1600 K and between 1700–1800 K, respectively. We then locate the temperature at which closure actually takes place. We note that crystals with voids of radii 0.6, 0.8, 1.0, and 1.5 nm disintegrate at 1380, 1460, 1580, and 1750 K, respectively. In Fig. 4, we also show the snapshots of the titanium crystal with 1.0 nm void at different time steps and at 1580 K. The closure of the void is clearly observed from this snapshot.

B. Void closure mechanism

Changes in the void volume, surface area, and the number of atoms are plotted as a function of time in Fig. 5. Voids with 0.6 and 0.8 nm radii fill differently than the 1.0 and 1.5 nm void. In the

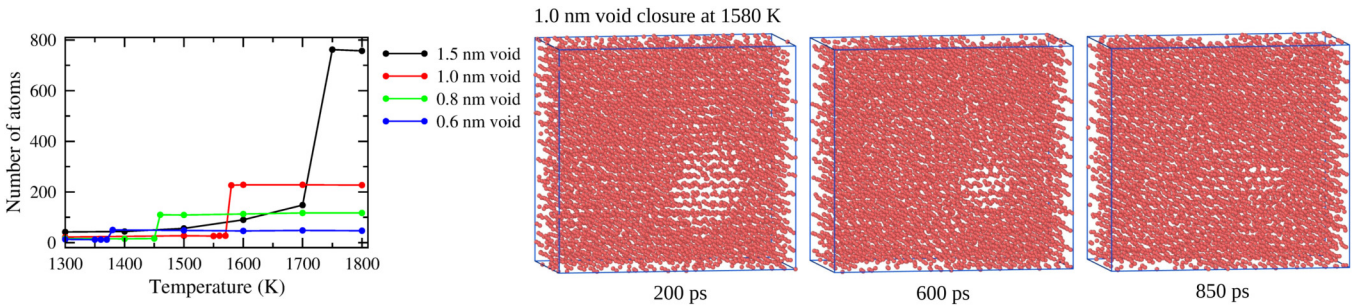

FIG. 4. Void filling as a function of temperature and snapshots of 1.0 nm void closure at 1580 K and at different timesteps.

former, the surface crumbles and atoms fill the void immediately. Surface simply crumbles at 100 and 400 ps for the 0.6 and 0.8 nm void, respectively. If we compare our findings for these two voids with Figs. 2 and 3, we observe that for these two systems, voids fill, but the crystal remains hcp till it melts. However, for the 1.0 nm void, it fills with three different rates. During the first 300 ps, the void retains it surface, then for the next 200 ps, the surface area reduces fast, and finally for next 400 ps, the void surface changes gradually. For all these voids, when the surface and volume reach some threshold, all of them collapses sharply. Unless this threshold is reached, atoms at the surface rearrange and hold it. We also plot the Lindemann index, Q_6 and coordination number as a function of time at these specific temperatures for the atoms only in the first layer. Interestingly, all these structural quantities for these atoms do not change even when the 0.6 and 0.8 nm void disappear. But for the atoms at the layer of 1.0 and 1.5 nm there is a change in these properties after 800 and 600 ps. However, within 10 ps of this change, Lindemann index stabilizes and Q_6 increases. Comparing both void properties and the first layer properties, we note that even when the voids fill, the atoms of the first layer maintain their crystallinity. For undercoordinated atoms at the surface coordination increases after the closure, but they order themselves like in crystal. It must be noted that all these local structural quantities are sensitive to minor changes in the immediate neighborhood of the atoms.

To further understand this re-arrangement, we plot the bond-orientational order parameter, coordination number, polyhedra properties, and the velocity auto-correlation functions for the first layer atoms of all these voids before and after the closure as a function of temperature. We plot them in Figs. 6 and 7. These local properties are obtained for the surface atoms with their neighbors lying within the first cut-off of the RDF. In Fig. 6, we note that both coordination number and polyhedra properties of the first layer of atoms change significantly when the voids fill. Thereafter, as the crystals are heated further, there is hardly any change in them. Even though these properties change when the voids close,

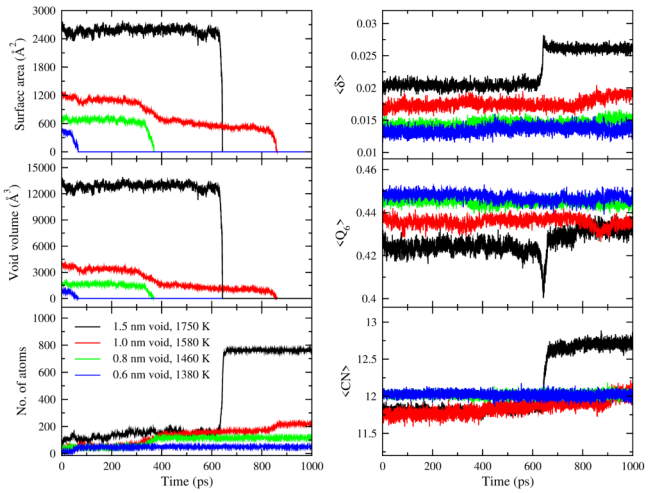

FIG. 5. Void volume, surface area, and number of atoms as a function of time. Lindemann index (δ), Q_6 order parameter, and coordination number of the first layer atoms' in 1.5, 1.0, 0.8, and 0.6 nm void as a function of time.

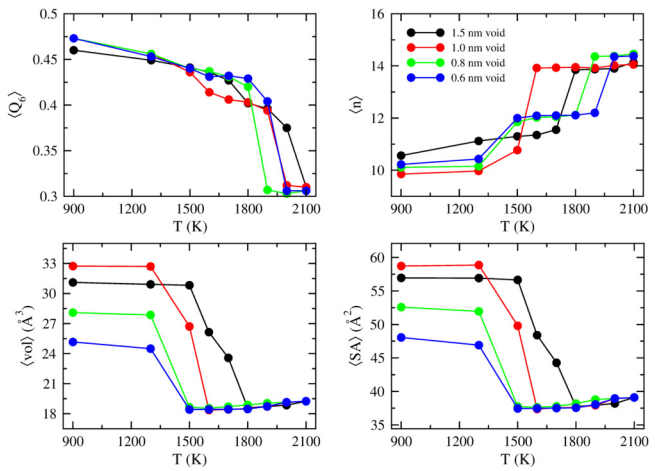

FIG. 6. Q_6 order parameter, coordination number, Voronoi volume, and surface area of first layer atoms on the void surface at different temperatures.

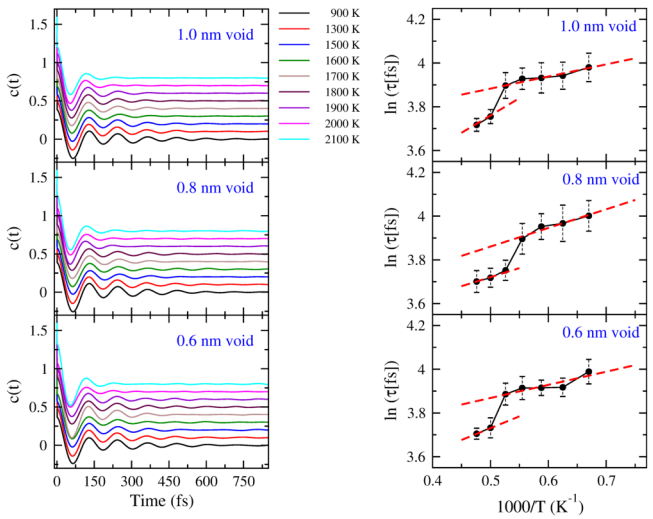

FIG. 7. Velocity autocorrelation function of the first layer of atoms on the void surface (left), relaxation times of velocity (right). Broken lines are Arrhenius fit to the data.

the bond-orientation order parameter of the first layer of atoms do not change.

Infact, the first layer of atoms undergoes minor changes till the crystal melts. This is true for all the voids wherein the bond-orientational order of the first layer changes between 2000–2100, 1900–2000, 1800–1900, and 1900–2000 K for 1.5, 1.0, 0.8, and 0.6 nm voids, respectively. Till these temperatures are attained, crystallinity is maintained even after the closure of the void. Surface atoms become a part of the crystal after the closure and arranges in an ordered manner. This is comparable with the RDF plots and other properties of these crystals reported in Figs. 2 and 3. Infact, the second peak of the RDF for 1.0 nm void crystal changes between 1500 and 1600 K. So for this crystal, the first layer hardly undergoes any change. Compared to orientational order, coordination numbers change differently. When coordination increases from 10 to 12, void fills (for all crystals), and when it increases from 12 to 14 (for 0.6 and 0.8 nm void) crystal melts. However, for the 1.5 and 1.0 nm the crystals' coordination number changes from 12 to 14 not necessarily mean melting of the crystal, rather the formation of 14 coordinated bcc atoms. These atoms are crystalline, which loses its order when heated further. We next discuss the polyhedra properties of the surface atoms.

Voronoi polyhedra are constructed by tessellating the space obtained by connecting the atoms surrounding the central atom. Its an important signature of void closure, which is also evident from this figure. As the void fills, the polyhedra volume and area change significantly. For both 0.6 and 0.8 nm void—it collapses between 1300 and 1500 K; consequently, there is a 20% decrease in Voronoi properties. As soon as the void disintegrate, there are atoms surrounding the surface atoms and, thus, polyhedra shrink. Interestingly, for the crystals with 1.0 and 1.5 nm void polyhedra properties change between 1300 and 1500 K and between 1500 and 1800 K respectively. These results clearly show the closure of the void, but it fails to distinguish between the bcc and liquid like surroundings of surface atoms. Differences between liquid and bcc atoms can be captured from the fraction of Voronoi indices $< n_3, n_4, n_5, n_6 >$ of polyhedra. In Fig. S11 in the supplementary material, we report these and observe that during the formation of bcc, there is a significant increase in $\langle 0, 6, 0, 8 \rangle$ polyhedra.

Velocity auto-correlation functions and relaxation times distinguish between correlations in liquid and solid. Atomic velocities in solid exhibit stronger correlations with longer relaxation times compared to liquid counterparts. We plot VACFs of the first layer of atoms in Fig. 7. Velocities of these atoms even when they become a part of the crystal are strongly correlated till the crystal melts. For the 0.6 nm void, strong correlations in velocities are observed till 1900 K, and similarly for the 0.8 nm void crystal, strong correlations exist till 1800 K. This validates our earlier findings that even after the voids fill, these crystals are hcp. We also obtain the relaxation times of these correlations. They change when the crystal melts. For the 1 nm void radius, correlations decrease between 1500 and 1600 K. However, they completely disappear between 1900 and 2000 K when the crystal melts. Relaxation times change when the crystals melt but not during the closure of the void.

IV. CONCLUSIONS

Melting of Ti crystals with different void radii are simulated here. Bulk thermodynamic properties and RDFs show that crystals with 0.6, 0.8, 1.0, and 1.5 nm void and void free crystal melts between 1900–2000, 1800–1900, 1900–2000, and 2000–2100 K, respectively. However, crystals with 1.0 and 1.5 nm spherical voids also show changes in these properties prior to its melting between 1500 and 1600 K and between 1700 and 1800 K. We find that these crystals change from hcp to bcc between these temperatures before it melts between 1900–2000 and 2000–2100 K. Thus, the hcp to bcc transition, which is, otherwise, not observed in straightforward MD simulations[47] is observed here for the 1.0 nm void crystal. Voids fill within 1 ps before crystals melt and this occur at 1380, 1460, 1580, and 1750 K for the 0.6, 0.8, 1.0, and 1.5 nm respectively. Bond-orientational order parameters and Voronoi properties also show that atoms of the first layer of the spherical void remains crystalline before and after void closes. Velocity auto-correlation functions further show that relaxation in these atoms are strongly correlated till the crystals melt. Local ordering in crystal is strongly correlated with the bulk thermodynamic properties of the crystal.

Compared to nucleating and non-nucleating mechanism,[10] reported earlier, we observe that surface atoms of the void remain crystalline before and after the closure when it mixes with other atoms. Interestingly, this is true for the crystal with 1.0 nm spherical void as well, where surface atoms rearrange to bcc before the entire crystal melts. This is different from the melting or stiffening of surface atoms during closure.[10] If we compare our findings here with our earlier results on copper,[23] we find that unlike copper where amorphization takes place before melting, here titanium remains crystalline till it melts. This is because of higher melting temperature and lower thermal conductivity of titanium compared to copper. Moreover, Ti crystal with the 1.0 nm void melts at a

temperature higher than the melting temperature of the 0.8 nm void crystal. However, copper crystal with 1.0 nm void melts at a lower temperature than the crystal with 0.8 nm void. Copper melts from the amorphous state, in Ti there is hcp to bcc transition before melting. This transition increases the melting of the Ti crystal with the 1.0 nm void.

Melting in crystals with high melting temperature and cohesive forces is very different from LJ systems or covalent solids like Si. Contrary to what is proposed in classical nucleation theory (CNT) that liquid like particles serve as nucleation sites, which then grows when the crystal melts, we observe that melting occurs when both long- and short-range orders disappear. Crystals when heated lose their long-range ordered arrangement and, finally, it melts when crystallinity within first shell atoms (short range) is completely lost. We show that even with spherical defects, melting occurs with the disappearance of order and there are no signs of liquid particles even at the surface of the 1.0 or 1.5 nm voids. Infact, these atoms also become crystalline after closure. Our findings further conclude that for Ti crystals with a spherical void of radius <1 nm, it fills up with heating spontaneously (within ps) and the crystal remains hcp, melting temperatures are comparable with the crystal without void. However, for the crystal with a spherical void of radius $\approx$ 1 nm, void closure changes hcp crystal to bcc and melting temperature also reduces. Our results will help to prepare and process titanium better for its several applications.

SUPPLEMENTARY MATERIAL

See the supplementary material for the plots of potential energies from the equilibration run, radial distribution function (RDF) of perfect hcp and bcc titanium at 300 K, and a-CNA diagram of the Ti crystal system with 1, 0.8, and 0.6 nm void during melting. It also includes the distribution of volume, surface area, faces, and edges of Voronoi polyhedra for all the systems including 1.5 nm void. Fraction of atoms and top ten Voronoi polyhedra for 1 nm void and the void free system are also reported.

ACKNOWLEDGMENTS

M.P.H. acknowledges Sikkim University for the fellowship. S.N.C. acknowledges Sikkim University for providing the computational facilities to perform the simulations.

AUTHOR DECLARATIONS

Conflict of Interest

The authors have no conflicts to disclose.

Author Contributions

Manash Protim Hazarika: Methodology (lead); Writing – original draft (equal). **Somendra Nath Chakraborty:** Conceptualization (lead); Supervision (lead); Writing – review & editing (lead).

DATA AVAILABILITY

The data that support the findings of this study are available from the corresponding author upon reasonable request.

REFERENCES

[1]N. Guo and M. C. Leu, Front. Mech. Eng. **8**, 215 (2013).
[2]R. R. Boyer, Mater. Sci. Eng. A **213**, 103 (1996).
[3]I. Gorynin, Mater. Sci. Eng. A **263**, 112 (1999).
[4]Q. Xu, W. Li, J. Zhou, Y. Yin, H. Nan, and X. Feng, Comput. Mater. Sci. **171**, 109280 (2020).
[5]P. Puri and V. Yang, J. Nanopart. Res. **11**, 1117 (2009).
[6]A. He, S. Duan, J.-L. Shao, P. Wang, and C. Qin, J. Appl. Phys. **112**, 074116 (2012).
[7]C. L. Williams, Metals **12**, 1667 (2022).
[8]X. Tian, H. Zhang, M. Xiang, and J. Cui, AIP Adv. **13**, 065027 (2023).
[9]X.-M. Bai and M. Li, Nano Lett. **6**, 2284 (2006).
[10]S. Li and W. Qi, J. Phys. Chem. C **119**, 6843 (2015).
[11]X.-T. Xu, F.-L. Tang, H.-T. Xue, W.-Y. Yu, L. Zhu, and Z.-Y. Rui, Comput. Mater. Sci. **107**, 58 (2015).
[12]Y. Qi, X. Chen, and M. Feng, J. Mater. Res. **34**, 3699 (2019).
[13]T. Tang, S. Kim, and M. Horstemeyer, Acta Mater. **58**, 4742 (2010).
[14]Y. Zhang, S. Jiang, X. Zhu, and Y. Zhao, Physica E **90**, 90 (2017).
[15]N. Amigo, Mol. Simul. **45**, 951 (2019).
[16]Y. Qi, X. Chen, and M. Feng, Mater. Sci. Eng. A **791**, 139444 (2020).
[17]T. Gao, H. Song, B. Wang, Y. Gao, Y. Liu, Q. Xie, Q. Chen, Q. Xiao, and Y. Liang, Int. J. Mech. Sci. **237**, 107800 (2023).
[18]J. Lutsko, D. Wolf, S. Phillpot, and S. Yip, Phys. Rev. B **40**, 2841 (1989).
[19]V. Van Hoang and T. Quy Dong, J. Chem. Phys. **136**, 104506 (2012).
[20]L.-B. Han, Q. An, R.-S. Fu, L. Zheng, and S.-N. Luo, J. Chem. Phys. **130**, 024508 (2009).
[21]W. Fan and X.-G. Gong, Phys. Rev. B **72**, 064121 (2005).
[22]L.-B. Han, Q. An, R.-S. Fu, L. Zheng, and S.-N. Luo, Physica B **405**, 748 (2010).
[23]M. P. Hazarika and S. N. Chakraborty, Chem. Phys. Lett. **730**, 521 (2019).
[24]P. M. Agrawal, B. M. Rice, and D. L. Thompson, J. Chem. Phys. **118**, 9680 (2003).
[25]H. Li, Z. Wen, and Q. Jiang, Solid State Commun. **147**, 250 (2008).
[26]F. Lindemann, Phys. Z **11**, 609 (1910).
[27]M. Born, J. Chem. Phys. **7**, 591 (1939).
[28]M. Volmer and A. Weber, Z. Phys. Chem. **119**, 277 (1926).
[29]R. Becker and W. Döring, Ann. Phys. **416**, 719 (1935).
[30]A. Samanta, M. E. Tuckerman, T.-Q. Yu, and W. E, Science **346**, 729 (2014).
[31]R. W. Cahn, Nature **323**, 668 (1986).
[32]R. Lipowsky, Phys. Rev. Lett. **49**, 1575 (1982).
[33]V. I. Levitas and K. Samani, Phys. Rev. B **89**, 075427 (2014).
[34]A. Basak and V. I. Levitas, Appl. Phys. Lett. **112**, 201602 (2018).
[35]J. Solca, A. J. Dyson, G. Steinebrunner, B. Kirchner, and H. Huber, Chem. Phys. **224**, 253 (1997).
[36]J. Solca, A. J. Dyson, G. Steinebrunner, B. Kirchner, and H. Huber, J. Chem. Phys. **108**, 4107 (1998).
[37]W. Petry, A. Heiming, J. Trampenau, M. Alba, C. Herzig, H. Schober, and G. Vogl, Phys. Rev. B **43**, 10933 (1991).
[38]K. Masuda-Jindo, S. Nishitani, and V. Van Hung, Phys. Rev. B **70**, 184122 (2004).
[39]Z.-G. Mei, S.-L. Shang, Y. Wang, and Z.-K. Liu, Phys. Rev. B **80**, 104116 (2009).
[40]D. Dickel, C. D. Barrett, R. L. Carino, M. I. Baskes, and M. F. Horstemeyer, Model. Simul. Mater. Sci. Eng. **26**, 065002 (2018).
[41]M. Poschmann, J. Lin, H. Geerlings, I. S. Winter, and D. Chrzan, Phys. Rev. Mater. **2**, 083606 (2018).
[42]J. Meiser and H. M. Urbassek, Metals **9**, 90 (2019).
[43]S. Plimpton, J. Comput. Phys. **117**, 1 (1995).
[44]M. S. Daw and M. I. Baskes, Phys. Rev. B **29**, 6443 (1984).
[45]G. J. Ackland, Philos. Mag. A **66**, 917 (1992).
[46]J. Jiang, X. Zhang, F. Ma, S. Dong, W. Yang, and M. Wu, Chem. Phys. Lett. **763**, 138187 (2021).

[47]M. I. Mendelev, T. Underwood, and G. Ackland, J. Chem. Phys. **145**, 154102 (2016).
[48]H. C. Andersen, J. Chem. Phys. **72**, 2384 (1980).
[49]S. Nosé, J. Chem. Phys. **81**, 511 (1984).
[50]W. G. Hoover, Phys. Rev. A **31**, 1695 (1985).
[51]L. Verlet, Phys. Rev. **159**, 98 (1967).
[52]A. Stukowski, Modell. Simul. Mater. Sci. Eng. **18**, 015012 (2009).
[53]M. Allen and D. Tildesley, *Computer Simulation of Liquids* (Oxford: Clarendon Press, 1987).
[54]H. H. Kart, H. Yildirim, S. O. Kart, and T. Çağin, Mater. Chem. Phys. **147**, 204 (2014).
[55]F. Ding, K. Bolton, and A. Rosén, Eur. Phys. J. D **34**, 275 (2005).
[56]P. J. Steinhardt, D. R. Nelson, and M. Ronchetti, Phys. Rev. B **28**, 784 (1983).
[57]W. Lechner and C. Dellago, J. Chem. Phys. **129**, 114707 (2008).
[58]C. Kuiying, L. Hongbo, L. Xiaoping, H. Qiyong, and H. Zhuangqi, J. Phys.: Condens. Matter **7**, 2379 (1995).
[59]T. T. Debela, X. Wang, Q. Cao, D. Zhang, and J. Jiang, J. Phys.: Condens. Matter **29**, 185401 (2017).
[60]S. N. Chakraborty, E. M. Grzelak, B. C. Barnes, D. T. Wu, and A. K. Sum, J. Phys. Chem. C **116**, 20040 (2012).
[61]W. C. Swope and H. C. Andersen, Phys. Rev. B **41**, 7042 (1990).
[62]G. Ruocco, M. Sampoli, and R. Vallauri, J. Chem. Phys. **96**, 6167 (1992).
[63]A. Idrissi, I. Vyalov, M. Kiselev, M. V. Fedorov, and P. Jedlovszky, J. Phys. Chem. B **115**, 9646 (2011).
[64]F. W. Starr, S. Sastry, J. F. Douglas, and S. C. Glotzer, Phys. Rev. Lett. **89**, 125501 (2002).
[65]C. H. Rycroft, "Multiscale modeling in granular flow," Ph.D. thesis (Massachusetts Institute of Technology, 2007).
[66]E. A. Lazar, Model. Simul. Mater. Sci. Eng. **26**, 015011 (2017).
[67]A. Stukowski, Model. Simul. Mater. Sci. Eng. **20**, 045021 (2012).
[68]J. D. Honeycutt and H. C. Andersen, J. Phys. Chem. **91**, 4950 (1987).
[69]D. Faken and H. Jónsson, Comput. Mater. Sci. **2**, 279 (1994).
[70]S.-P. Pan, S.-D. Feng, J.-W. Qiao, W.-M. Wang, and J.-Y. Qin, Sci. Rep. **5**, 16956 (2015).
[71]C. Chakravarty, P. G. Debenedetti, and F. H. Stillinger, J. Chem. Phys. **126**, 204508 (2007).